Clim. Past Discuss., 9, 6429–6458, 2013
www.clim-past-discuss.net/9/6429/2013/
doi:10.5194/cpd-9-6429-2013

Climate of the Past
Discussions
Open Access

Comparing modelled fire dynamics with charcoal records for the Holocene

T. Brücher[1], V. Brovkin[1], S. Kloster[1], J. R. Marlon[2], and M. J. Power[3]

[1]Max Planck Institute for Meteorology, Hamburg, Germany
[2]School of Forestry and Environmental Studies, Yale University, New Haven, CT, USA
[3]Natural History Museum of Utah, Department of Geography, University of Utah, Salt Lake City, UT 84112, USA

Received: 28 October 2013 – Accepted: 10 November 2013 – Published: 27 November 2013

Correspondence to: T. Brücher (tim.bruecher@mpimet.mpg.de)

Published by Copernicus Publications on behalf of the European Geosciences Union.

Abstract

An Earth System model of intermediate complexity, CLIMBER-2, and a land surface model JSBACH that represents vegetation dynamically are used to simulate natural fire dynamics through the last 8000 yr. Output variables of the fire model (burned area and fire carbon emissions) are used to compare model results with sediment-based charcoal reconstructions and several approaches of model output processing are tested. Charcoal data are reported in Z-scores and have been used for the period 8000 to 200 BP to exclude the post-Industrial period of strong anthropogenic forcing during the last two centuries. The model-data comparison reveals a robust correspondence in fire trends for most regions considered, while few regions, such as Europe, display different trends between simulated and observed trends. The difference between the modelled and observed fire activity could be linked to an absence of the anthropogenic forcing (e.g., human ignitions and suppression) in the model simulations, but also related to limitations of model assumptions for modelling fire dynamics. For the model trends, the usage of spatial averaging or Z-score processing of model output resulted in similar directions of trend. However, modelled Z-scores resulted in higher rank correlations with the charcoal Z-scores in most of the regions. Therefore, while both metrics are useful, the Z-score processing is more preferable for the modelled fire comparison with the charcoal records than the areal averaging.

1 Introduction

The current interglacial period, the Holocene, that started about 11 800 cal yr BP, is characterized by relatively stable climate. The main trends of changing climate and environment are assumed to follow slow changes in the orbital forcing. The maximum of incoming summer solar irradiance in the Northern Hemisphere was about 11 thousand years ago higher by app. 50 W m^{-2} (65° N: 528.45 W m^{-2} at 11 000 cal yr BP; Berger, 1978; Berger et al., 1998; Tzedakis et al., 2012), but until about 9,000 cal yr BP years

CPD
9, 6429–6458, 2013

ago the climate in the northern temperate and high latitude regions was affected by remains of the Northern Hemisphere ice sheets. Based on terrestrial proxy records, a time slice of 6 000 cal yr BP was chosen as a reference mid-Holocene period for the Paleo Model Intercomparison project (PMIP, Braconnot et al., 2007).

Because ample records of climate and environmental changes are available for the Holocene (e.g., Wanner et al., 2008), this period is a well-suited to test climate and biospheric models and compare these results with the syntheses of geological archives (e.g., BIOME6000). Simulated and reconstructed changes in climate and vegetation cover (e.g., Claussen, 1997; Kutzbach and Liu, 1997) have often been compared to the 6,000 cal yr BP time slice. More recently, the palaeo modelling research has focused on simulating transient changes, for example, in the sea surface temperature (Lorenz et al., 2006), sea ice (Fischer and Jungclaus, 2010), land surface climate (Renssen et al., 2004), and comparison of available pollen records with the tree cover changes (Kleinen et al., 2011). Progress in the synthesis of the Holocene land cover and land use changes (e.g., Gaillard et al., 2010) and climate proxy records (Marcott et al., 2013) now provides a basis for detailed model-data comparison throughout the Holocene period.

Fire is an important process that affects climate through changes in CO_2 emissions, albedo, and aerosols (Ward et al., 2012), as well as the disturbance of vegetation cover (Sitch et al., 2003). Fire-history reconstructions from charcoal accumulations in sediment have indicated that biomass burning has increased since the Last Glacial Maximum (Power et al., 2008; Marlon et al., 2013). Recent comparisons with transient climate model output suggest that this increase in global fire activity is linked primarily to variations in temperature and secondarily to variations in precipitation (Daniau et al., 2012). A new aspect of the recent generation of Earth System Models (ESM) is the implementation of fire models (Arora and Boer, 2005; Kloster et al., 2010; Thonicke et al., 2010; Pfeiffer et al., 2013) that allow testing hypotheses generated through reconstructions of palaeofire data on the controls of fire across a range of spatial and temporal scales. Fire model outputs have included simulated burned areas and CO_2 emissions

CPD
9, 6429–6458, 2013

that can be evaluated against present day observations from remote sensing products. For example, Kloster et al. (2010) demonstrated that the Arora and Boer (2005) fire model implemented in the Community Land Model (CLM-CN) reproduces reasonable patterns and annual cycles of burned area and carbon emissions within the range of satellite based observations. Simulated mean burned area (327 $Mha\,yr^{-1}$) was at the lower band of satellite observations (329 to 401 $Mha\,yr^{-1}$), and modelled carbon emissions varied between 2.0 to 2.4 $Pg\,C\,yr^{-1}$, also close to the low end of satellite products (2.3 to 2.7 $Pg\,C\,yr^{-1}$).

Recent progress in the analysis and syntheses of charcoal records led to a Global Charcoal Database with hundreds of records from around the world (Power et al., 2008; Daniau et al., 2012). To analyse the temporal changes in the charcoal database, individual charcoal records are transformed and standardized to allow comparisons across the multiple types of records (e.g., Power et al., 2008; Marlon et al., 2009; Daniau et al., 2012; Marlon et al., 2013). The standardization allows analysis of trends in different regions using charcoal records obtained from a wide range of depositional environments and quantified with different laboratory techniques.

In this study we use the advantages offered from a mechanistic model and ask "What factors are causing the variations in fire?" and will analyse how well fire models reproduce reconstructed trends in fire activity during the last 8000 yr and ask "How well can fire models reproduce reconstructed trends in fire activity?". From a methodological perspective, we ask "What is the best way to compare fire model output with charcoal records?". The last question is important because (i) the fire model provides quantitative information about burned area and fire-related emissions of CO_2, but charcoal-based palaeofire data only provide information about relative changes in biomass burning, and (ii) since the charcoal records are interpreted via a non-linear power transformation, the model can be used to determine whether, for example, a 2× increase in the standardized charcoal reconstruction reflects a 2×, 200×, or some other increase in area burned. The essential steps in answering these questions are to test how well the model can reproduce the reconstructions, develop metrics for characterizing the

CPD
9, 6429–6458, 2013

comparisons, and to understand how the data transformation and standardization affects the model output.

In the following, Sect. 2 describes the data and model used in this study in detail, including the transformation and standardization of model output to Z-scores. Section 3 discusses the driver of variation, comparison of model results and charcoal data on (i) large (continental) and (ii) regional (sub-continental) spatial scales followed by a summary of key findings in Sect. 4.

2 Methods

2.1 Charcoal reconstructions

The Global Charcoal Database (GCD version 2.5) is used to determine regional and global palaeofire trends from 218 sedimentary charcoal records covering part or all of the last 8000 yr. To retrieve regional and global composites of changes in fire activity over the Holocene, charcoal accumulation in sediments is compiled and transformed (Power et al., 2008; Marlon et al., 2009) as a standardized measure frequently used by the palaeofire community to compare aggregated values of past fire activity. The transformation aims to homogenize the variance within individual time series using a Box–Cox transformation, and then rescales the values and calculating anomalies to identify time periods of lower- and higher-than-modern fire activity. Modern is usually defined as a time window prior to the Industrial period. The Box–Cox transformation is necessary, as reconstructions of charcoal records are based on a wide range of processing techniques and various types of sites and differ by several orders of magnitude. The Z-score transformation is based on three major steps: (1) rescaling values using a minimax transformation; (2) homogenization of variance using the Box–Cox transformation; and (3) rescaling values once more to Z-scores. The Z-score transformation is applied to each time series ci_s of charcoal influxes ci for each site “s” separately. First, the linear minimax transformation ci'_s (Eq. 1) is used to scale the values ci_s between 0 and 1, by

CPD
9, 6429–6458, 2013
Comparing modelled fire dynamics with charcoal records for the Holocene
T. Brücher et al.

subtracting the minimum value $\min(ci_s)$ and divide by the amplitude $(\max(ci_s) - \min(ci_s))$ of the time series.

$$ci'_s = \frac{ci_s - \min(ci_s)}{\max(ci_s) - \min(ci_s)} \tag{1}$$

The non-linear Box–Cox transformation ci^*_s (Eq. 2) reduces high numbers and removes outliers to achieve a more Gaussian-like distribution (e.g., Fig. 3 in Power et al., 2008):

$$ci^*_s = \begin{cases} \frac{(ci'_s+\alpha)^{\lambda_s}-1}{\lambda_{s},} & \lambda_s \neq 0 \\ \log(ci'_s + \alpha) & \lambda_s = 0 \end{cases} \tag{2}$$

Here, the parameter λ_s is estimated by a maximum-likelihood method (Venables and Ripley, 1994) for each time series at each charcoal site "s" separately. To avoid a division by zero, a small constant α is added (here: $\alpha = 0.01$). Afterwards, the minimax and Box–Cox transformed time series ci^*_s (Eq. 2) is normalized by subtracting the mean value of a predefined base period $\overline{ci^*_s}$ and dividing the anomalies by the standard deviation $S^*_{ci_s}$ of the minimax and Box–Cox transformed time series ci^*_s (Eq. 2):

$$ci^Z_s = \frac{ci^*_s - \overline{ci^*_s}}{S_{ci^*_s}} \tag{3}$$

To retrieve regional, aggregated values Z_{region} out of the site information ci^Z_s (Eq. 3), all time series ci^Z_s are linearly averaged (Eq. 4) by deviding with the number of sites (N_{sites}):

$$Z_{\text{region}} = \sum_{\text{sites}} \frac{ci^Z_s}{N_{\text{sites}}} \tag{4}$$

Discussion Paper | Discussion Paper | Discussion Paper | Discussion Paper |

CPD
9, 6429–6458, 2013

Comparing modelled fire dynamics with charcoal records for the Holocene

T. Brücher et al.

Even though the Z-score transformation is not linear it is still rank conserving. In order to calculate area composites, each record was sampled (without interpolation) at 20 yr intervals and afterwards smoothed (lowess) by running a 250 yr moving window. Furthermore, a bootstrap analysis (sampling by site) was used to obtain the 95 % confidence intervals for the Z-score of a region.

2.1.1 CLIMBA – a fast global carbon cycle model

The computational efficiency of ESMs is rather low, therefore it is a challenge to do interactive simulations over the Holocene, as, for example, done by Fischer and Jungclaus (2010). Furthermore, most of these studies do not include an interactive carbon cycle. Combining a model of intermediate complexity with a land model of full complexity bridges the gap between long simulations and computational efficiency on the quality of the simulated climate. For this study, we developed a new coupled climate-carbon cycle model CLIMBA. It consists of the earth system model of intermediate complexity (EMIC) CLIMBER-2 (Petoukhov et al., 2000; Ganopolski et al., 2001) and JSBACH (Reick et al., 2013; Schneck et al., 2013; Brovkin et al., 2009; Raddatz et al., 2007), which is the land component of the Max-Planck-Institute Earth System Model (MPI-ESM; Giorgetta et al., 2013). While CLIMBER-2 simulates the atmosphere and land processes at roughly 51° (longitude) by 10° (latitude), the JSBACH model runs on higher spatial resolution (3.75° longitude by 3.75° latitude) including a daily cycle to better resolve heterogeneous land processes. The coupling procedure between CLIMBER and JSBACH is analogue to the coupling described in Kleinen et al. (2010). As base climate daily values of MPI-ESM CMIP5 simulation for the early industrial period (here defined as 1850–1899) are used. The JSBACH module is driven by climate anomalies (w.r.t. the base climate) from CLIMBER-2 added on a randomly chosen year out of the 50 yr spanning base climate. As CLIMBER-2 does not simulate year-to-year climate variability, this coupling approach ensures variability at this timescale within the forcing for JSBACH, which is critical for simulating fire in JSBACH. Because the base climate is chosen from the pre-industrial simulation, the year-to-year variability is given

CPD
9, 6429–6458, 2013

by the variability of the base climate alone. The climate forcing includes values for temperature, precipitation, radiation balance, and atmospheric CO_2 concentration. Given this climate and orbital forcing, JSBACH runs offline for one model-year. The simulated change in the total land carbon feeds back to CLIMBER-2 as a carbon flux to the atmosphere (negative or positive) and closes the carbon cycle.

JSBACH includes a dynamical vegetation scheme and calculates disturbance of vegetation by natural fire occurrence and windthrow. While the default JSBACH version (Reick et al., 2013) uses a simple fire module (Brovkin et al., 2009), the fire algorithm used in this study is based on (Arora and Boer, 2005), which simulates fire occurrence as a function of fuel availability, fuel moisture, and ignition source (Kloster et al., 2010, 2013; Krause et al., 2013). The fire model calculates a potential burned area, which is simulated as a function of moisture and wind speed. The associated carbon emissions are calculated as a function of area burned and available fuel load. There is no distinction whether carbon emits as CH_4 or CO_2.

Kloster et al. (2010) shows, that the Arora and Boer (2005) algorithm implemented in the Community Land Model (CLM-CN) reproduces reasonable patterns and annual cycles of burned area and carbon emissions within the range of satellite based observations.

In this study we keep lightning constant while recognizing it is a weather-driven process and therefore variable within the changing climate of the Holocene. We also do not account for human ignitions and anthropogenic land use or anthropogenic land cover changes and acknowledge these factors can impact the carbon cycle. Therefore, the research focus is designed to explore potential vegetation and natural fire occurrence.

2.2 Experimental setup

A transient simulation spanning 8000 yr has been performed starting at the mid Holocene at 8000 cal yr BP (8 ka = 8000 cal yr BP; 0 ka = 1950 AD). The initial conditions are taken from a control simulation with CLIMBA for cal yr BP with an atmospheric CO_2 concentration of 260 ppm, in accordance with the reconstruction from ice core (Elsig

CPD
9, 6429–6458, 2013

et al., 2009). The transient simulation includes an orbital forcing after Berger (1978), fixed greenhouse gases and aerosol concentration, and ignores changes in sea level and land ice. At the end of the transient simulation, atmospheric CO_2 concentration is simulated as 272 ppm, which is lower than observed by app. 8 ppm (Monnin et al., 2004). In an additional simulation we included land use emissions (e.g., Pongratz et al., 2009; Ruddiman, 2003) by an additional land atmosphere carbon flux after a scenario based on Hyde (Goldewijk, 2001). In this scenario the atmospheric CO_2 concentration at pre-industrial (PI) times is higher by 18 ppm. As the focus on this study is on natural vegetation and natural fire occurrence, these land use emissions are neglected.

Reconstructions and model data are restricted to between 8000 cal yr BP and 200 cal yr BP to exclude the start of industrialization period and the large human impact on fire activity during the subsequent centuries. Furthermore, within this period the charcoal database has the most number and highest sample density of palaeofire records and therefore the highest data quality.

2.3 Processing of model output for the comparison with charcoal data

For the comparison with reconstructions of palaeofire, two output variables of the fire model at each grid box g have been used: (1) the fraction of grid box area burned per year f_g [yr^{-1}] and (2) the total carbon flux to the atmosphere c_g [$\mathrm{g\,C\,m^{-2}\,yr^{-1}}$]. To compare aggregated model results of burned area (F) and carbon emissions (C) with regional estimates of fire activity out of the charcoal database reported as Z-scores (Z), the model output is processed using two different approaches: (i) At time t the grid box values $f_g(t)$ and $c_g(t)$ related to the region under investigation are weighted by its

CPD
9, 6429–6458, 2013
Comparing modelled fire dynamics with charcoal records for the Holocene
T. Brücher et al.

area a_g [m^2] and summed up to get accumulated, regional numbers (Eqs. 5 and 6):

$$F_{region}(t) = \sum_g f_g(t) \cdot a_g \quad (5)$$

$$C_{region}(t) = \sum_g c_g(t) \cdot a_g \quad (6)$$

(ii) Furthermore, Z-score transformed (Eq. 3) time series f_g^z and c_g^z are derived from f_g and c_g of each grid box. Then they are linearly averaged to achieve regional time series of burned area F_{region}^z and carbon emissions C_{region}^z (Eqs. 7 and 8). Without using an area weighting function the local information of vegetated area get lost by just dividing with the number of grid boxes per region N_g:

$$F_{region}^Z(t) = \frac{\sum_g f_g^Z(t)}{N_g} \quad (7)$$

$$C_{region}^Z(t) = \frac{\sum_g c_g^Z(t)}{N_g} \quad (8)$$

These two different approaches of absolute values (Eqs. 5 and 6) and regional averaged Z-scores (Eqs. 7 and 8) of model output are used in the following.

To reduce the high year-to-year variability, a 250 yr running mean filter is applied before the Z-scores are derived. For reconstructions and model data, the used Box–Cox transformation and the normalization afterwards are based on the full period (7800 yr), in particular the same period is used to calculate the mean and standard deviation used in Eq. (3). Hence, charcoal influxes and model output are treated in the same way to minimize inconsistencies in the statistical analysis and maximize comparability. Therefore, regional disparities in the model-data comparison cannot be explained by differences in data processing.

CPD
9, 6429–6458, 2013

3 Results and discussion

3.1 Changes in fire activity at 8000 cal yr BP

The natural variability and trends in fire occurrence simulated by the model are driven by changes in climate and climate induced changes in vegetation cover. We discuss in the following the simulated changes in fire occurrence in conjunction with changes in precipitation and temperature as the dominant drivers for vegetation and fire activity. Furthermore, we will investigate the agreement on modelled and observed palaeofire reconstructions and then focus the discussion on the advantages of transforming the model results in to aggregated Z-score time series.

During the mid-Holocene, the Northern Hemisphere received more solar irradiation during the summer season relative to pre-industrial (Berger, 1978). This led to substantial summer warming which was most pronounced in high northern latitudes (Renssen et al., 2009). Northern subtropics, including North Africa, were substantially wetter, presumably due to an intensification of the monsoon circulation. This led to the significant increase of vegetation cover in subtropical drylands and in the Sahel/Sahara region (Prentice et al., 1992; Claussen, 1997). While the Northern Hemisphere was warmer over the Holocene, the temperature anomalies in southern extra-tropics (30–60° S) were small (Wanner et al., 2008). These general features of the mid-Holocene climate changes are well reproduced by the CLIMBER-2 model as also seen by previous studies (e.g., Claussen, 1997). Temperature anomalies simulated by the CLIMBER-2 model on a yearly mean basis are within the range of $-0.5\,^{\circ}$C to $0.5\,^{\circ}$C except the area of the West African and Indian Monsoon with a strong dipole of a cooler, wetter region and a warm area (not shown).

Our simulated total burned area (Figs. 1a and 3a) for the mid Holocene is at 514 Mha yr^{-1} and increases slightly by 14 Mha yr^{-1} (app. 2.5 %) to 528 Mha yr^{-1}. The hotspots of burned area are located in tropical Africa, central North America, central

CPD
9, 6429–6458, 2013

South America, Australia and partly the Mediterranean region plus South Asia. The increase until 200 cal BP is mainly due to more fire in the Amazon, North America, South Asia, and the East Coast of Australia (Fig. 1b). The main regions of a decrease in fire activity (burned area fraction) are tropical West Africa, Central Australia, and Europe (Fig. 1b). Looking at carbon emissions (Fig. 1c), the pattern is similar to the pattern of burned area (Fig. 1a) capturing similar hot spots of palaeofire activity (note, the scale of the color bars differ by a factor 1000). An increase of almost 5 % (0.29 Gt C yr^{-1}) is calculated by the transient simulation. This trend in carbon emissions appears stronger than trends in burned area. Although, there are some regions (e.g., central South Africa) showing a decrease in burned area along with an increase in carbon emissions. Compensating effects of declining burned area, but a higher vegetation fraction (Fig. 2b) along with more carbon in living biomass due to the atmospheric CO_2 fertilization could explain these opposing trends. Regions with an increasing higher burned area but decreasing carbon emissions linked to natural fire do not by JSBACH.

To understand the temporal evolution of regional fire occurrence Hovmöller diagrams of anomalies (8000 cal yr BP minus 200 cal yr BP) are shown (Fig. 2) for precipitation (Fig. 2a), desert fraction (Fig. 2b), carbon in living biomass (Fig. 2c), and burned area fraction (Fig. 2d; note, this is land data only). In general, the patterns of anomalies do not identify strong gradients with time, even before applying the 250 yr smoothing window. So, there are no abrupt changes with time simulated, however, the latitudinal gradient does identify some sharp boundaries, which are likely an effect of the coarse resolution of the 10° latitudinal bands of CLIMBER-2 anomalies driving the land model JSBACH.

There are two dominant patterns of anomalies apparent: within the northern tropics the intensified and northward shifted monsoon system (Fig. 3a) during the Holocene leads to a wide spread greening (Fig. 3b) with an increased biomass (Fig. 3c) between 8000 cal yr BP and 4000 cal yr BP as previously observed by Prentice et al. (e.g., 1992); Claussen (e.g., 1997); Brovkin et al. (e.g., 2002). Because of the humid climate in the

Discussion Paper | Discussion Paper | Discussion Paper | Discussion Paper |

CPD
9, 6429–6458, 2013

Comparing modelled fire dynamics with charcoal records for the Holocene

T. Brücher et al.

northern tropics, decreases in fire activity become amplified with time. Therefore, we suggest the trend in fire activity is climate driven and not determined by fuel.

The second prominent pattern lies around 20–30° S, where zonal means of yearly precipitation point to drier conditions at 8000 cal yr BP to 6,000 cal yr BP. For South Africa, all but the southern tip was drier during 8000 cal yr BP, as the monsoon system shifted northward (Fig. S1a). For South America a dipole of drier Amazonia and a wetter region south of 20° S is simulated (Fig. S1b). Therefore the small increase (up to 100 mm yr^{-1}) in annual precipitation in Australian almost counterbalances on latitudinal means the decrease of precipitation in South America. Between 20° S and 30° S, the vegetated area increases over the whole period, while there is no prominent shift in the zonal averaged numbers of green biomass. The increase in vegetated area parallels the increase in fire activity. This trend is apparent because of the higher fire occurence in South America and Africa, while a modelled dipole of changes in burned area over Australia amplifies the trend at app. 20–30° S and lessens the increase south of 30° S.

For the northern extra tropics, the patterns are noisier (Figs. 1 and 2) and an overall prominent decline of the boreal forest is not as strong (Figs. 2a and S1g) as expected after e.g. Claussen (1997) and Kleinen et al. (2010). The increased vegetated area at app. 60° N can mainly be linked to some greening spots in Asia and Alaska without impacting the fire activity.

3.2 Comparison of simulated and reconstructed trends in fire activities

3.2.1 Comparison on hemispheric scale

To compare the modelled and reconstructed numbers of aggregated Z-score values on hemispheric scale we investigate five spatial domains separately: global [90° S–90° N] (Fig. 3a), northern extra tropics [90–30° N] (Fig. 3b), northern tropics [30–0° N] (Fig. 3c), southern tropics [0–30° S] (Fig. 3d), and southern extra tropics [30–90° S] (Fig. 3e). These domains are chosen in analogue to Daniau et al. (2012). Shown are

CPD
9, 6429–6458, 2013

Z-score transformed time series of reconstructed (charcoal influx, Z) and modelled (burned area F^Z and carbon emissions C^Z) fire activity. There is also the untransformed model output of burned area (F) given, as well as the number of sites the reconstructions are based on. The untransformed figures for carbon emissions by fire (C) are not shown, as on regional to hemispheric scale F and C are almost linearly correlated (not shown here). Charcoal data are given as the median and the ±95th percentile of a bootstrap analysis (see Sect. 2.1). A large spread between median and the ±95th percentile highlights a low number of records in the database or a heterogeneous domain (e.g., Fig. 3c). For three different time periods (8000 cal yr BP–PI, 8000 cal yr BP–4000 cal yr BP, 4000 cal yr BP–PI) the rank correlation after Spearman (1908) is used as an objective measure to quantify the agreement between modelled and reconstructed values. The numbers are given for the correlations between (i) Z and $F(\rho(Z,F))$, (ii) Z and $F^Z(\rho(Z,F^Z))$, and (iii) Z and $C^Z(\rho(Z,C^Z))$ as a bar chart next to the global or large scale zonal averages.

On global scale (Fig. 3a) an increase within the burned area is observed (red line = burned area). With a base of 218 sites, the spread between the ±95th percentiles and the median is rather low, suggesting that the global signal out of the reconstructions is rather robust. Modelled data do agree in the trend and magnitude (14 Mha, app. 2.5 %). If the same fire model is used within an earth system model, findings by Krause et al. (2013) suggest values in the same order of magnitude (app. 580 Mha burned area per year) by counting for present day climate, pre-industrial land areas and no human ignition. However, if the fire model is used in a more realistic setup for present day climate (Kloster et al., 2010), a mean simulated burned area of 327 Mha yr^{-1} stays at the lower band of satellite observations from 329 Mha yr^{-1} (GFED) to 401 Mha yr^{-1} (L4JRC). Model results of carbon emissions vary between 2.0 to 2.4 Pg C yr^{-1} and are close to the numbers of satellite products (2.3 to 2.7 Pg C yr^{-1}). While the rank correlation between the untransformed model data is small ($\rho(Z,F) = 0.18$), the numbers are much higher ($\rho(Z,F^Z) = 0.73$ and $\rho(Z,C^Z) = 0.77$) if the Z-scores of charcoal values are compared to Z-scores of modelled burned area. If the full period of 7800 yr is divided into two subsets (8000 cal yr BP to 4000 cal yr BP and 4000 cal yr BP to PI), the correlation is reduced, especially for the latter one, which suggests the overall Holocene trend is reproduced, but not the sub-millennial variability. The decrease in fire can be related to drier conditions on a global scale. While changes in temperature are relatively small (app. 0.1 K, see Fig. S2a), decreases in yearly precipitation by app. 40 mm yr^{-1} and the small increase in biomass (w.r.t. fuel availability) dominate the effect on driving fire activity. The continuous increase in the carbon stocks is also be supported by CO_2 fertilization (12 ppm increase; Fig. S2a; Keenan et al., 2013).

For the northern extra tropics the charcoal data show a small increase, while the modelled fire activity stays almost constant (Fig. 3b) at app. 164 Mha. A rank correlation gives a negative correlation coefficient for the Z-scores of burned area and carbon emissions with the charcoal reconstructions, while the correlation of burned area and the charcoal reconstructions is not significant (Fig. 3b). On the large area mean, the temperature decreases by 0.2 K, the climate gets drier (40 mm yr^{-1}), and the biomass decreases. The shift toward reduced fuel availability and drier conditions seems to be compensated by drier conditions, which lead to almost no change in modelled burned area.

For the tropics (Fig. 3c and d) a strong increase in burned area is reported after 7000 cal yr BP in the charcoal database. The model results reflect this increase over the full period and all time series are positively correlated, ranging from $\rho(Z, F^Z) = 0.42$ to $\rho(Z, C^Z) = 0.48$ (for further details see Table S1). While the numbers of Z-score transformed data suggest a strong change, the modelled numbers vary only by 6 Mha from 8000 cal yr BP to PI (northern and southern tropics), which suggests a change by roughly 4 %. In the case of untransformed modelled data, the correlation shrinks by factor of three, which supports the standardization of model output to improve comparability with charcoal influx values. In terms of large-scale averages, climate is not changing significantly over the 7800 yr in the southern tropics, while precipitation decreases in the northern tropics by app. 10 %. (80 mm yr^{-1}). As precipitation is the controlling parameter for tropical vegetation, biomass decreases in the northern tropics

CPD
9, 6429–6458, 2013

and increases slightly in the southern tropics. As both areas point toward an increase in fire activity, it seems that on a large scale fire in the tropics is primarily determined by fuel abundance and moisture availability.

For the southern extra tropics (Fig. 3e) the level of reconstructed natural fire activity stays almost constant with a small decrease around 4000 cal yr BP. However, the model results show a strong increase in burned area and carbon emissions over the entire period of 7800 yr simulated. The rank correlation shows, that less than 15 % of variability is explained by the Z-score transformed data ($\rho(Z, FZ) = 0.24$; $\rho(Z, C^Z) = 0.22$) and the absolute, not transformed values of burned area do not correlate significantly ($p < 0.05$) with the reconstructions. An explanation for the disagreement could be the small land area in general and a large fraction of coastal area within this region (southern part of Africa, Patagonia, and partly Australia), which are in general difficult to represent in global climate models. Alternatively, the domain of southern extra tropics is the area with the highest simulated burned area (nearly 70 %). However, the simulated drop in temperature (by 0.2 K) is rather small, but the decrease in precipitation, leading to drier conditions, appears more significant. Since the vegetated fraction on the landscape is not significantly increasing, the higher values of Z-score burned area are likely linked to changes in precipitation.

In general, the trend of simulated burned area and their carbon emissions point to a small increase in fire occurence, which is reflected in the observed charcoal reconstructions as well. The regional correlation analysis explains a maximum of 25 % of the variance for the different areas. Running the correlation analysis for the two time segments (8000 cal yr BP to 4000 cal yr BP and 4000 cal BP to 200 cal yr BP) separately, the correlation decreases or even becomes negative, which suggests that the general trend of increasing burned area over the entire period (8000 cal yr BP until 200 cal yr BP) is partly reproduced and responsible for the correlation coefficient over the 7800 yr.

The simulation discussed above is redone three times to get an ensemble of four members. All members are started with the same restart, but as the a member of the base climate is chosen randomly (see Sect. 2.1.1) all simulations do develop independently. The analysis of the ensemble shows that the simulated trends in fire occurance are robust (Fig. S2).

3.2.2 Comparison on regional scale

To investigate the model performance on more homogeneous regions, the methodology used in the previous Sect. 3.2.1 is applied on regional scale, following domains defined and discussed in Marlon et al. (2013) (Figs. 4 and 5). Most of the charcoal Z-score time series point to an increase in fire activity, except Central America tropics (Fig. 4c), where a u-shaped pattern of Z-score influxes comes across with a high centennial variability including a high uncertainty possibly caused by a low number of charcoal records available ($n = 9$). The Asia monsoon region (Fig. 4f) also has a limited number of charcoal records ($n = 10$).

On a first glance, JSBACH simulates an increase in all regions except Europe (Fig. 4b), where a decrease between 6,000 cal yr BP and 4000 cal yr BP is simulated and afterwards the burned area and carbon emissions remain at lower levels. In terms of numerical output, the simulated decrease in fire is about one quarter (6 Mha) of the total and modelled values stay at 18 Mha for PI climate (Fig. S4b). It can also be seen, that for all regions the modelled timing of local minima or maxima does not match the reconstructions. Running the rank correlation on these time series, the overall agreement in an increase of fire activity points to positive correlation coefficients between $\rho = 0.32$ and $\rho = 0.66$ ($p < 0.05$). The highest number is found for reconstructed charcoal influxes and modelled carbon emissions by wildfire in North America (Fig. 4a), which is also the region with the most charcoal data available. The charcoal reconstructions for Africa (Fig. 4d) fit the model results rather well ($\rho = 0.46$; $p < 0.001$), even though the charcoal database contains a limited number of records for that region. When the correlation is divided into two time periods (8000 cal yr BP to 4000 cal yr BP and 4000 cal yr BP to PI), the explained variance decreases, and the results indicate negative values (Fig. 5). The only exception is provided by the African region (Fig. 4d and 5), where the correlation coefficient between the Z-scores of modelled carbon emissions and charcoal influxes increases from $\rho = 0.46$ ($p < 0.001$) for the entire time period to $\rho = 0.61$ ($p < 0.001$) for the earlier sub-period (8000 cal yr BP to 4000 cal yr BP), but turns negative for the later time interval. Interestingly, the modelled burned area decreases with time slightly, but the Z-score transformed values show an opposite trend by a clear increase in carbon emissions and burned area. In general, the transformed time series for each grid box differ in the scaling, but not in the trend or sign. As Z-score-transformation removes the absolute value of the variable, averaging several transformed grid cells can change the sign of the trend. As an example, two neighboring grid boxes with one showing an increase by 50 % and the other showing a decrease by 50 % of fire activity, can result in a Z-score of zero. If the boxes, however, differ in their burned area magnitude the absolute change would be different from zero or similar to the average for the base period.

Another unique result for Africa (Fig. 4d) is the interplay between burned area and carbon emissions. While in all hemispheric regions (Fig. 3) and continental-scale regions (Fig. 4) the correlation coefficient between Z-scores of modelled burned area and modelled carbon emissions is at minimum $\rho = 0.98$ ($p < 0.001$; Table S1), although the values are much lower ($\rho = 0.84, p < 0.001$) for the African region.

By considering significant and positive rank correlations, we find for all regions – except Central America tropics (Fig. 4c) – a higher rank correlation between Z-score transformed data and reconstructions ($\rho(Z,F^Z)$ and $\rho(Z,C^Z)$), than for untransformed model data and reconstructions ($\rho(Z,F)$). Taking the model setup of this study the main driver for changes in Holocene climate (last 8000 yr) is given by the orbital forcing and changes due to increasing CO_2 are of secondary order. Please note, human impact in the experimental setup is neglected. Furthermore, this study focuses on large, heterogeneous regions and therefore differences in the results based on (Z,C^Z) vs. (Z,F^Z) are minor. Looking at the ensemble results (Fig. S4), it is apparent, that the trends simulated by each ensemble member are rather close to each other and differences between the model results and reconstructions are systematic.

CPD
9, 6429–6458, 2013

4 Conclusions

Running a fast global carbon cycle model over the Holocene until pre-industrial times (here defined as 200 yr before 1950 AD) a transient climate change is simulated close to reconstructed patterns from proxy records. With the focus on the capability to simulate reconstructed trends in natural fire activity, different regions on continental to regional scale were compared to Z-score transformed charcoal influx data. Close to the overall increase in fire activity out of charcoal reconstructions we simulate a total increase of app. 14 Mha (from 512 to 526 Mha) for burned area. The increase itself and the variability on millennial timescales vary between and among regions. The absolute numbers are high, as the human dimension in terms of fire ignitions and fire suppression is neglected. In addition, the model counts for fire activity given by a potential natural vegetation (no land use and land use cover change included).

One limiting component of our model setup is the choice of an EMIC as the climate driver. Especially on regional scale, our fire model results are limited by the quality of the climate forcing, what can (partly) explain the not reproduced centennial or millennial variability. In comparison to the results shown here, a further model study by Kloster et al. (2013) supports this conclusion: Kloster et al. (2013) gets different simulated trends on regional scale (Europe and North America) over the Holocene (6000 cal yr BP to PI) due to a different climate forcing out of a transient simulation (MPI-ESM) with constant atmospheric CO_2 concentration.

For most of the investigated regions the model simulates an increase in burned area and carbon emissions. The trends in the carbon emissions were higher than trends detected in burned area. We propose several reasons for this observation: (i) CO_2 fertilization by the increasing atmospheric CO_2 concentration increases the emissions per square meter burned area due to higher carbon stock in the vegetation. (ii) The carbon stock of the fuel increases due to changes in the fuel types. This could be due to the dynamical vegetation changes or due to changes in the fire occurrence due to climate changes. A rank correlation analysis points to the overall agreement between simulated

CPD
9, 6429–6458, 2013

and observed trends in fire activity over the whole period of study, while a rank correlation on sub time segments shows, that the model does not match the centennial- or millennial-scale variability. An agreement on variability on these timescales is not expected, as regional climate affects local fire activity, and there is no reason why the timing of the modelled climate variability should coincide with the climate of the past. The differences and similarities between reconstructions and model results are stable. The analysis of an four member ensemble shows rather small differences between the individual simulations and a consistent trend given by the ensemble members (Figs. S4 and S5).

From a modelling perspective, this study helps to validate the capability of a model to simulate past fire activity. On the other side, as the fire model is not tuned by reconstruction data, the overall agreement (on hemispheric and regional scale) shows the high quality of the Global Charcoal Database. Even regions which are sparse covered by reconstructions correlate with the model results, therefore to some degree the fire model can be used to fill the missing spatial information.

Z-score transformed data do not inform about a quantitative change in burned area, as the transformation is rank conserving, but not linear. So, neither a given change within the Z-score values does not mean an increase or decrease by the same percentage change, nor the range of fluctuations informs about the magnitude of changes, which could lead to different trends, if we consider regional averages of transformed or un-transformed data. Therefore, it is useful to convert the time series of modelled burned area or carbon emissions to Z-score to provide a method for comparing modelled and observed palaeofire variability. While we do see some general agreement between model results and reconstructions, it is still open if the absolute values of simulated burned area are capturing the right magnitude for past fire activity. While high fluctuations could suggest huge changes (e.g., Fig. 4e), the absolute change is rather small (2 Mha, app. 7 %). Future studies should consider methods of transforming model output variables and palaeo proxy data consistently to increase the comparability of simulated and observed data. In this study the Z-score transformation helps to

CPD
9, 6429–6458, 2013

validate modelled natural fire occurrence and compare it to reconstructed values of charcoal influxes reported as Z-scores.

Supplementary material related to this article is available online at http://www.clim-past-discuss.net/9/6429/2013/cpd-9-6429-2013-supplement.pdf.

Acknowledgements. We thank data contributors to the Global Charcoal Database and members of the Global Palaeofire Working Group (GPWG). We also thank Gitta Laaslop for discussing the paper, Veronika Gayler and Reiner Schnur for their technical support. This work was supported by funding to the Past4Future project from the European Commission's 7th Framework Programme, grant number 243908, and is Past4Future contribution number 59.

The service charges for this open access publication have been covered by the Max Planck Society.

References

Arora, V. K. and Boer, G. J.: Fire as an interactive component of dynamic vegetation models, J. Geophys. Res, 110, G02008, doi:10.1029/2005JG000042, 2005. 6431, 6432, 6436

Berger, A.: Long-term variations of daily insolation and Quaternary climatic changes, J. Atmos. Sci., 35, 2362–2367, 1978. 6430, 6437, 6439

Berger, A., Loutre, M. F., and Gallée, H.: Sensitivity of the LLN climate model to the astronomical and CO_2 forcings over the last 200 ky, Clim. Dynam., 14, 615–629, 1998. 6430

Braconnot, P., Otto-Bliesner, B., Harrison, S., Joussaume, S., Peterchmitt, J.-Y., Abe-Ouchi, A., Crucifix, M., Driesschaert, E., Fichefet, Th., Hewitt, C. D., Kageyama, M., Kitoh, A., Laîné, A., Loutre, M.-F., Marti, O., Merkel, U., Ramstein, G., Valdes, P., Weber, S. L., Yu, Y., and Zhao, Y.: Results of PMIP2 coupled simulations of the Mid-Holocene and Last Glacial Maximum – Part 1: experiments and large-scale features, Clim. Past, 3, 261–277, doi:10.5194/cp-3-261-2007, 2007. 6431

Brovkin, V., Bendtsen, J., Claussen, M., Ganopolski, A., Kubatzki, C., Petoukhov, V., and Andreev, A.: Carbon cycle, vegetation, and climate dynamics in the Holocene: experiments with the CLIMBER-2 model, Global Biogeochem. Cy., 16, 1139, doi:10.1029/2001GB001662, 2002. 6440

Brovkin, V., Raddatz, T., Reick, C., Claussen, M., and Gayler, V.: Global biogeophysical interactions between forest and climate, Geophys. Res. Lett, 36, L07405, doi:10.1029/2009GL037543, 2009. 6435, 6436

Claussen, M.: Modeling bio-geophysical feedback in the African and Indian monsoon region, Clim. Dynam., 13, 247–257, 1997. 6431, 6439, 6440, 6441

Daniau, A.-L., Bartlein, P. J., Harrison, S. P., Prentice, I. C., Brewer, S., Friedlingstein, P., Harrison-Prentice, T. I., Inoue, J., Izumi, K., Marlon, J. R., Mooney, S., Power, M. J., Stevenson, J., Tinner, W., Andrič, M., Atanassova, J., Behling, H., Black, M., Blarquez, O., Brown, K. J., Carcaillet, C., Colhoun, E. A., Colombaroli, D., Davis, B. A. S., D'Costa, D., Dodson, J., Dupont, L., Eshetu, Z., Gavin, D. G., Genries, A., Haberle, S., Hallett, D. J., Hope, G., Horn, S. P., Kassa, T. G., Katamura, F., Kennedy, L. M., Kershaw, P., Krivonogov, S., Long, C., Magri, D., Marinova, E., McKenzie, G. M., Moreno, P. I., Moss, P., Neumann, F. H., Norström, E., Paitre, C., Rius, D., Roberts, N., Robinson, G. S., Sasaki, N., Scott, L., Takahara, H., Terwilliger, V., Thevenon, F., Turner, R., Valsecchi, V. G., Vanniere, B., Walsh, M., Williams, N., and Zhang, Y.: Predictability of biomass burning in response to climate changes, Global Biogeochem. Cy., 26, GB4007, doi:10.1029/2011GB004249, 2012. 6431, 6432, 6441

Elsig, J., Schmitt, J., Leuenberger, D., Schneider, R., Eyer, M., Leuenberger, M., Joos, F., Fischer, H., and Stocker, T. F.: Stable isotope constraints on Holocene carbon cycle changes from an Antarctic ice core, Nature, 461, 507–510, 2009. 6436

Fischer, N. and Jungclaus, J. H.: Effects of orbital forcing on atmosphere and ocean heat transports in Holocene and Eemian climate simulations with a comprehensive Earth system model, Clim. Past, 6, 155–168, doi:10.5194/cp-6-155-2010, 2010. 6431, 6435

Gaillard, M.-J., Sugita, S., Mazier, F., Trondman, A.-K., Broström, A., Hickler, T., Kaplan, J. O., Kjellström, E., Kokfelt, U., Kuneš, P., Lemmen, C., Miller, P., Olofsson, J., Poska, A., Rundgren, M., Smith, B., Strandberg, G., Fyfe, R., Nielsen, A. B., Alenius, T., Balakauskas, L., Barnekow, L., Birks, H. J. B., Bjune, A., Björkman, L., Giesecke, T., Hjelle, K., Kalnina, L., Kangur, M., van der Knaap, W. O., Koff, T., Lagerås, P., Latałowa, M., Leydet, M., Lechterbeck, J., Lindbladh, M., Odgaard, B., Peglar, S., Segerström, U., von Stedingk, H., and

CPD
9, 6429–6458, 2013

Comparing modelled fire dynamics with charcoal records for the Holocene

T. Brücher et al.

Seppä, H.: Holocene land-cover reconstructions for studies on land cover-climate feedbacks, Clim. Past, 6, 483–499, doi:10.5194/cp-6-483-2010, 2010. 6431
Ganopolski, A., Petoukhov, V., Rahmstorf, S., Brovkin, V., Claussen, M., Eliseev, A., and Kubatzki, C.: CLIMBER-2: a climate system model of intermediate complexity, Part II: Model sensitivity, Clim. Dynam., 17, 735–751, 2001. 6435
Goldewijk, K. K.: Estimating global land use change over the past 300 years: the HYDE database, Global Biogeochem. Cy., 15, 417–433, 2001. 6437
Keenan, T. F., Hollinger, D. Y., Bohrer, G., Dragoni, D., Munger, J. W., Schmid, H. P., and Richardson, A. D.: Increase in forest water-use efficiency as atmospheric carbon dioxide concentrations rise, Nature, 499, 324–327, 2013. 6443
Kleinen, T., Brovkin, V., von Bloh, W., Archer, D., and Munhoven, G.: Holocene carbon cycle dynamics, Geophys. Res. Lett, 37, L02705, doi:10.1029/2009GL041391, 2010. 6435, 6441
Kleinen, T., Tarasov, P., Brovkin, V., Andreev, A., and Stebich, M.: Comparison of modeled and reconstructed changes in forest cover through the past 8000 years: Eurasian perspective, Holocene, 21, 723–734, 2011. 6431
Kloster, S., Mahowald, N. M., Randerson, J. T., Thornton, P. E., Hoffman, F. M., Levis, S., Lawrence, P. J., Feddema, J. J., Oleson, K. W., and Lawrence, D. M.: Fire dynamics during the 20th century simulated by the Community Land Model, Biogeosciences, 7, 1877–1902, doi:10.5194/bg-7-1877-2010, 2010. 6431, 6432, 6436, 6442
Kloster, S., Brücher, T., Brovkin, V., and Wilkenskjeld, S.: Controls on fire activity over the Holocene: fuel availability versus fuel moisture, Geophys. Res. Lett., in preparation, 2013. 6436, 6447
Krause, A., Kloster, S., Wilkenskjeld, S., and Paeth, H.: Lightning and wildfires: past, present, future, J. Geophys. Res., submitted, 2013. 6436, 6442
Kutzbach, J. E. and Liu, Z.: Response of the African monsoon to orbital forcing and ocean feedbacks in the middle Holocene, Science, 278, 440–443, 1997. 6431
Lorenz, S. J., Kim, J.-H., Rimbu, N., Schneider, R. R., and Lohmann, G.: Orbitally driven insolation forcing on Holocene climate trends: evidence from alkenone data and climate modeling, Paleoceanography, 21, PA1002, doi:10.1029/2005PA001152, 2006. 6431
Marcott, S. A., Shakun, J. D., Clark, P. U., and Mix, A. C.: A reconstruction of regional and global temperature for the past 11 300 years, Science, 339, 1198–1201, 2013. 6431
Marlon, J. R., Bartlein, P. J., Walsh, M. K., Harrison, S. P., Brown, K. J., Edwards, M. E., Higuera, P. E., Power, M. J., Anderson, R. S., and Briles, C.: Wildfire responses to abrupt

CPD
9, 6429–6458, 2013

climate change in North America, P. Natl. Acad. Sci. USA, 106, 2519–2524, 2009. 6432, 6433

Marlon, J. R., Bartlein, P. J., Daniau, A.-L., Harrison, S. P., Maezumi, S. Y., Power, M. J., Tinner, W., and Vanniére, B.: Global biomass burning: a synthesis and review of Holocene paleofire records and their controls, Quaternary Sci. Rev., 65, 5–25, 2013. 6431, 6432, 6457

Monnin, E., Steig, E. J., Siegenthaler, U., Kawamura, K., Schwander, J., Stauffer, B., Stocker, T. F., Morse, D. L., Barnola, J.-M., Bellier, B., Raynaud, D., and Fischer, H.: Evidence for substantial accumulation rate variability in Antarctica during the Holocene, through synchronization of CO_2 in the Taylor Dome, Dome C and DML ice cores, Earth Planet. Sc. Lett., 224, 45–54, 2004. 6437

Petoukhov, V., Ganopolski, A., Brovkin, V., Claussen, M., Eliseev, A., Kubatzki, C., and Rahmstorf, S.: CLIMBER-2: a climate system model of intermediate complexity, Part I: Model description and performance for present climate, Clim. Dynam., 16, 1–17, 2000. 6435

Pfeiffer, M., Spessa, A., and Kaplan, J. O.: A model for global biomass burning in preindustrial time: LPJ-LMfire (v1.0), Geosci. Model Dev., 6, 643–685, doi:10.5194/gmd-6-643-2013, 2013. 6431

Pongratz, J., Reick, C. H., Raddatz, T., and Claussen, M.: Effects of anthropogenic land cover change on the carbon cycle of the last millennium, Global Biogeochem. Cy., 23, GB4001, doi:10.1029/2009GB003488, 2009. 6437

Power, M., Marlon, J., Ortiz, N., Bartlein, P., Harrison, S., Mayle, F., Ballouche, A., Bradshaw, R., Carcaillet, C., and Cordova, C.: Changes in fire regimes since the Last Glacial Maximum: an assessment based on a global synthesis and analysis of charcoal data, Clim. Dynam., 30, 887–907, 2008. 6431, 6432, 6433, 6434

Prentice, I. C., Cramer, W., Harrison, S. P., Leemans, R., Monserud, R. A., and Solomon, A. M.: Special paper: a global biome model based on plant physiology and dominance, soil properties and climate, J. Biogeogr., 117–134, 1992. 6439, 6440

Raddatz, T. J., Reick, C. H., Knorr, W., Kattge, J., Roeckner, E., Schnur, R., Schnitzler, K.-G., Wetzel, P., and Jungclaus, J.: Will the tropical land biosphere dominate the climate–carbon cycle feedback during the twenty-first century?, Clim. Dynam., 29, 565–574, 2007. 6435

Reick, C. H., Raddatz, T., Brovkin, V., and Gayler, V.: Representation of natural and anthropogenic land cover change in MPI-ESM, J. Adv. Model. Earth Syst., 5, 1–24, doi:10.1002/jame.20022, 2013. 6435, 6436

Renssen, H., Goosse, H., Fichefet, T., Brovkin, V., Driesschaert, E., and Wolk, F.: Simulating the Holocene climate evolution at northern high latitudes using a coupled atmosphere-sea ice-ocean-vegetation model, Clim. Dynam., 24, 23–43, 2004. 6431

Renssen, H., Seppä, H., Heiri, O., Roche, D., Goosse, H., and Fichefet, T.: The spatial and temporal complexity of the Holocene thermal maximum, Nat. Geosci., 2, 411–414, 2009. 6439

Ruddiman, W. F.: The anthropogenic greenhouse era began thousands of years ago, Climatic Change, 61, 261–293, 2003. 6437

Schneck, R., Reick, C. H., and Raddatz, T.: Land contribution to natural CO_2 variability on time scales of centuries, J. Adv. Model. Earth Syst., 5, 354–365, 2013. 6435

Sitch, S., Smith, B., Prentice, I. C., Arneth, A., Bondeau, A., Cramer, W., Kaplan, J. O., Levis, S., Lucht, W., and Sykes, M. T.: Evaluation of ecosystem dynamics, plant geography and terrestrial carbon cycling in the LPJ dynamic global vegetation model, Glob. Change Biol., 9, 161–185, 2003. 6431

Spearman, C.: The method of "right and wrong cases" ("constant stimuli") without Gauss's formulae, Brit. J. Psychol., 1904–1920, 2, 227–242, 1908. 6442

Thonicke, K., Spessa, A., Prentice, I. C., Harrison, S. P., Dong, L., and Carmona-Moreno, C.: The influence of vegetation, fire spread and fire behaviour on biomass burning and trace gas emissions: results from a process-based model, Biogeosciences, 7, 1991–2011, doi:10.5194/bg-7-1991-2010, 2010. 6431

Tzedakis, P. C., Channell, J. E. T., Hodell, D. A., Kleiven, H. F., and Skinner, L. C.: Determining the natural length of the current interglacial, Nat. Geosci., 5, 138–141, 2012. 6430

Venables, W. N. and Ripley, B. D.: Modern Applied Statistics with S-PLUS, New York u.a. Springer (2007), 4 Edn., ISBN:9780387954578, 465–480, 1994. 6434

Wanner, H., Beer, J., Bütikofer, J., Crowley, T. J., Cubasch, U., Flückiger, J., Goosse, H., Grosjean, M., Joos, F., Kaplan, J. O., Küttel, M., Müller, S. A., Prentice, I. C., Solomina, O., Stocker, T. F., Tarasov, P., Wagner, M., and Widmann, M.: Mid- to Late Holocene climate change: an overview, Quaternary Sci. Rev., 27, 1791–1828, 2008. 6431, 6439

Ward, D. S., Kloster, S., Mahowald, N. M., Rogers, B. M., Randerson, J. T., and Hess, P. G.: The changing radiative forcing of fires: global model estimates for past, present and future, Atmos. Chem. Phys., 12, 10857–10886, doi:10.5194/acp-12-10857-2012, 2012. 6431

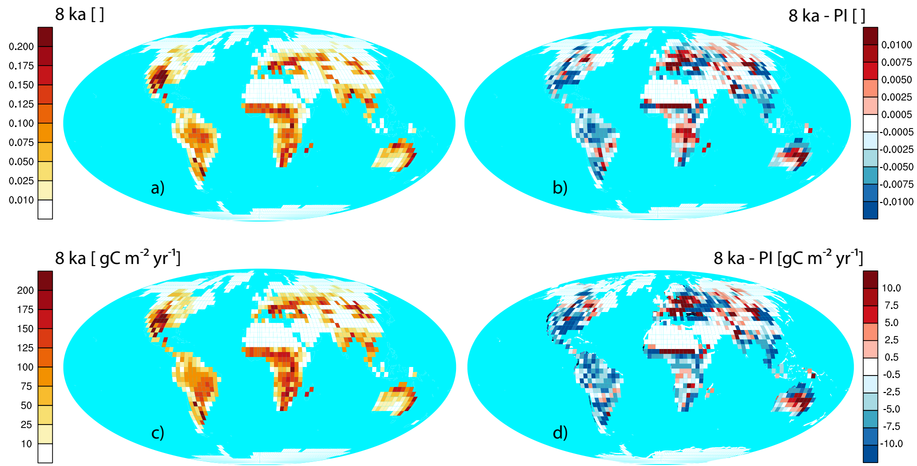

Fig. 1. Yearly burned fraction of grid cell area [$m^2\,m^{-2}$] of natural fire activity **(a)** and carbon emissions [$g\,C\,m^{-2}\,yr^{-1}$] **(c)** for the mid-Holocene (8 ka = 8000 cal yr BP) and their anomalies **(b, d)** to burned fraction with pre-industrial (PI = 200 cal yr BP) climate.

CPD
9, 6429–6458, 2013

Comparing modelled fire dynamics with charcoal records for the Holocene

T. Brücher et al.

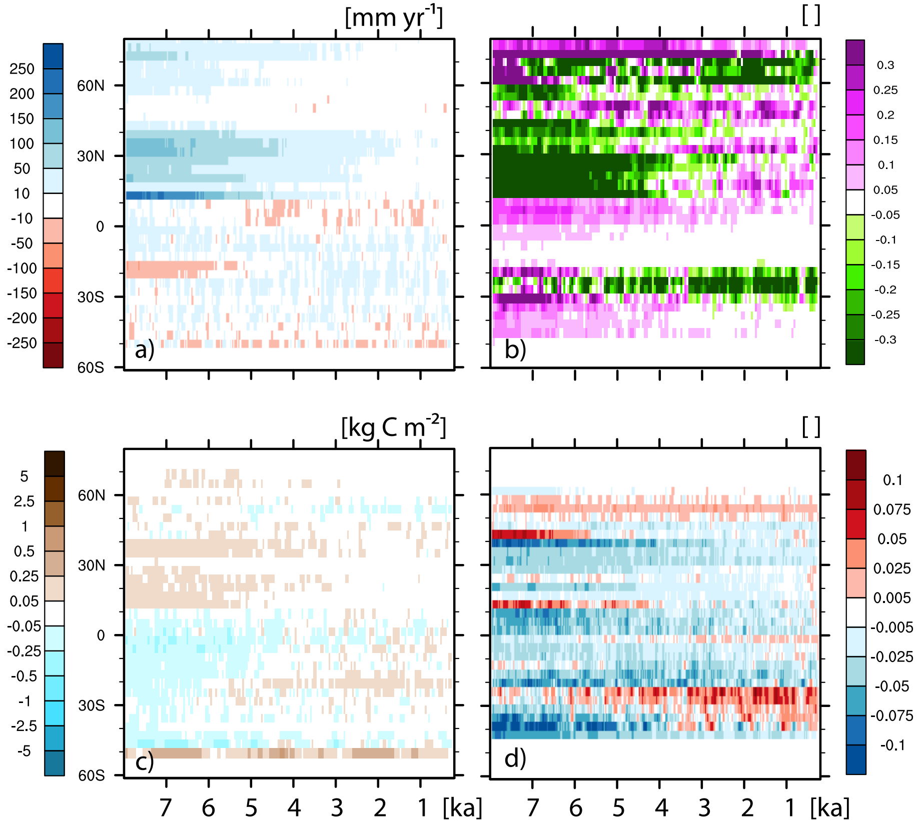

Fig. 2. Transient anomalies of latitudinal averaged values (over land) for **(a)** yearly precipitation [mm yr^{-1}], **(b)** desert fraction [m^2 m^{-2}], **(c)** carbon [kg C m^{-2}] stored in green biomass, and **(d)** fraction of burned area [m^2 m^{-2}]. The base period for calculating all anomalies is pre-industrial climate (PI).

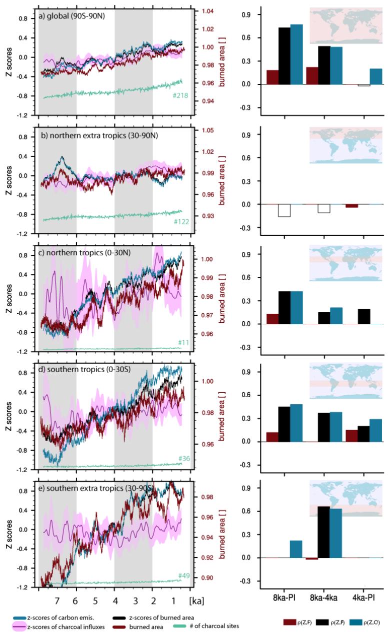

Fig. 3. Averaged values for reconstructed and modelled biomass burning during the present interglacial as global values **(a)**, for extra tropics (**b** and **e**), and tropics (**c** and **d**) separately. Reconstructions are shown by Z-scores of charcoal influxes (Z, pink), and Z-score transformed values of modelled burned area (F^Z, black) and carbon emissions by fire (C^Z, blue). Untransformed model output of burned area (F, red) and the number of sites used in the reconstructions (green) are also given. For all time series a running mean of 250 yr is applied. Please note the varying, relative scale of modelled burned area. The scale for the modelled Z-scores of burned area is determined by the maximum amplitude of Z-score transformed charcoal influxes (reconstructions). On the right side, the corresponding rank correlations ρ (after Spearman) are shown. Significant, positive values are given by filled bars for three different time windows: 8 ka–PI, 8 ka–4 ka, and 4 ka–PI.

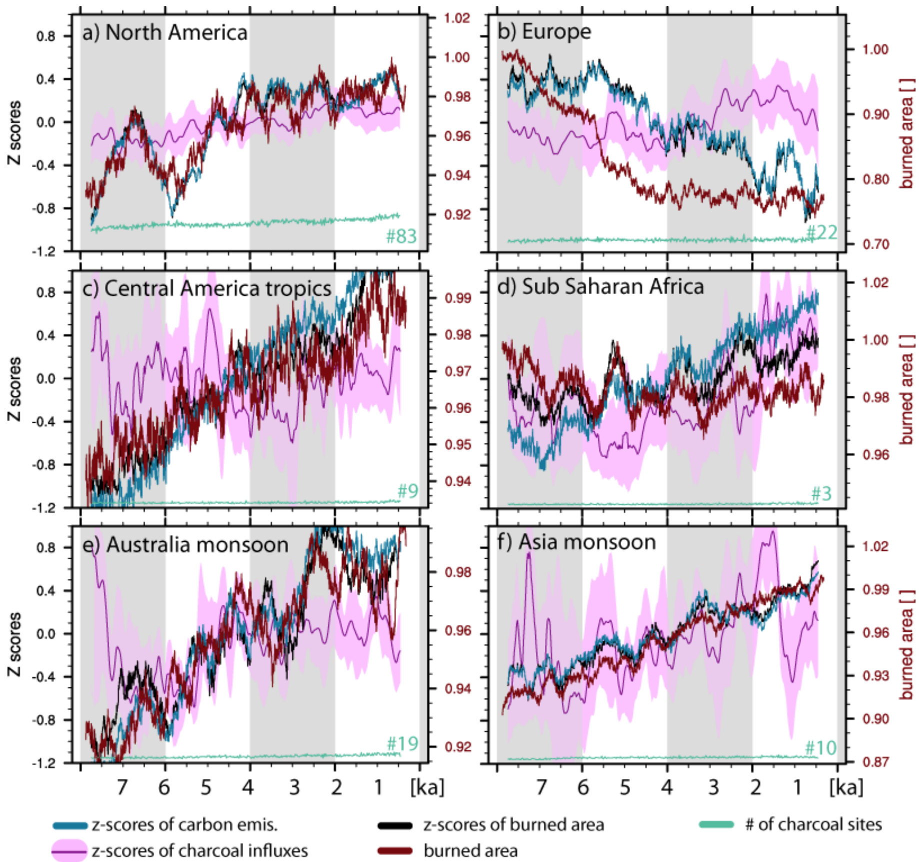

Fig. 4. Same as Fig. 3, but for continental scale regions North America **(a)**, Europe **(b)**, Central America tropics **(c)**, Sub Saharan Africa **(d)**, Australian monsoon region **(e)**, and Asia monsoon region **(f)**. The definition of the domains is taken from Marlon et al. (2013). For the rank correlations see Fig. 5.

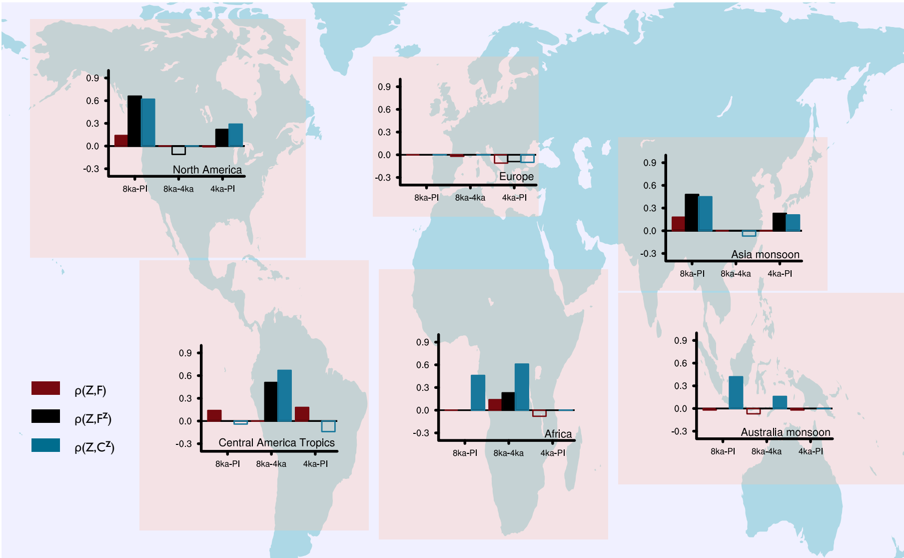

Fig. 5. Regional rank correlations ρ (after Spearman) are shown (compare Fig. 4). Significant, positive values are given by filled bars for three different time windows: 8 ka–IP, 8 ka–4 ka, and 4 ka–PI. The underlying, aggregated time series are shown in Fig. 4.

CPD
9, 6429–6458, 2013

Comparing modelled fire dynamics with charcoal records for the Holocene

T. Brücher et al.